The First X-ray Characterized Monosubstituted Ferrocenyl Azacrown Chalcone: Focus on Its Calcium Interaction/Electrochemical Detection Studies

Béatrice Delavaux-Nicot,*[a] Jérôme Maynadié,[a] Dominique Lavabre,[b] Christine Lepetit,[a] and Bruno Donnadieu[a,c]

Keywords: Calcium / Cations / Crown compounds / Ferrocene / Sensors

The first X-ray characterization of an azacrown ferrocenyl chalcone [$(C_5H_5)Fe(C_5H_4COCH{=}CHC_6H_4$-*p*-aza-15-crown-5)] (**2**) is reported. Its cation electrochemical detection capabilities have been evaluated and its behaviour towards protonation and calcium addition has been thoroughly examined. The uncommon ligand–Ca^{2+} interaction process involves three species of different stoichiometry in equilibrium in solution. Their association constants have been calculated. These species are formed by interaction of calcium with both the azacrown and CO functions of compound **2**, as evidenced by NMR and IR spectroscopy. The theoretical MESP analysis also suggests that, contrary to its *N*-ethyl-substituted homologue [$(C_5H_5)Fe(C_5H_4COCH{=}CHC_6H_4NEt_2)$] (**1a**), both coordination sites of **2** are involved in this interaction process. The study highlights that the CO group of **2** improves the selectivity of the cation electrochemical detection when compared to the known compound [$(C_5H_5)Fe(C_5H_4$-$CH{=}CHC_6H_4$-*p*-aza-15-crown-5)].

Introduction

Although a plethora of redox-active or fluorescent molecules have proved their usefulness as ion sensors,[1] ferrocenyl receptors that contain two types of signaling units, i.e. electroactive and fluorescent, are rare.[2] They could be the keystone of new families of ion chemo-sensors that can either sense different guests or display two or more macroscopic observable events upon addition of a certain analyte.[2c,3a] The fabrication of these systems and their integration into different supports (e.g. electronically conducting polymeric supports and optical fiber) would lead to novel prototype molecular sensory devices for commercial use.[1b,2a]

Recently, we have investigated the synthesis of electroactive receptors that combine a ferrocenyl unit and a purely organic fluorescent ion sensor subunit containing an R-amino complexing moiety (-$COCH{=}CHC_6H_4$-*p*-R):[2b] In particular, the disubstituted compound [$Fe(C_5H_4$-$COCH{=}CHC_6H_4NEt_2)_2$] behaves as a new type of multiresponsive calcium-sensing device in CH_3CN.[4] Its monosubstituted counterpart [$(C_5H_5)Fe(C_5H_4COCH{=}CHC_6H_4$-$NEt_2)$] (**1a**) is not fluorescent. However, interposition of the conjugated -$COCH{=}CHC_6H_4$- spacer between the ferrocene unit and the NEt_2 ionophore in this compound allows an electronic communication through the link.[2b] This important property suggests that molecules containing this fluorescent organic fragment could be electrochemical sensors. Other research teams have also shown a great deal of interest in the studies of related compounds (analogs of **1a**) incorporating a CO function directly linked to a ferrocenyl moiety,[5] and tested these compounds in applications such antimalarial activity[6] or as potential anticancer drugs.[7] However, none of these compounds was evaluated for electrochemical sensing.

In an earlier study,[8] we focused on the effect of the insertion of a -CH=CH- unit into the conjugated link of compound **1a**, and evaluated three *N*-alkyl ferrocenyl derivatives with a variable spacer length towards cation electrochemical detection (Scheme 1).

Redox-active ionophores based on covalently linked crown ether–metallocene systems have received much attention in recent years because they provide a good selective electrochemical response to the presence of a guest cation.[9] In the present study, we have investigated the influence of the substituent of the nitrogen atom on the cation electrochemical detection and have replaced the diethylamino group of **1a** by the aza-15-crown-5 residue to synthesize compound **2** (Scheme 2). Furthermore, we have pursued our interest in understanding and quantifying the nature of the complex process leading to the calcium electrochemical detection. To the best of our knowledge, this is not a

[a] Laboratoire de Chimie de Coordination du CNRS, UPR 8241, 205, route de Narbonne, F-31077, Toulouse cedex 04, France
Fax: +33-5-6155-3003
E-mail: delavaux@lcc-toulouse.fr
[b] Laboratoire des Interactions Moléculaires et Réactivité Chimique et Photochimique, UMR 5623 du CNRS, Université Paul Sabatier,
118 route de Narbonne, 31062, Toulouse cedex, France
[c] Present address: University of California, Riverside, Department of Chemistry,
324 Pierce Hall Building Riverside, CA 92521, USA
Supporting information for this article is available on the WWW under http://www.eurjic.org or from the author.

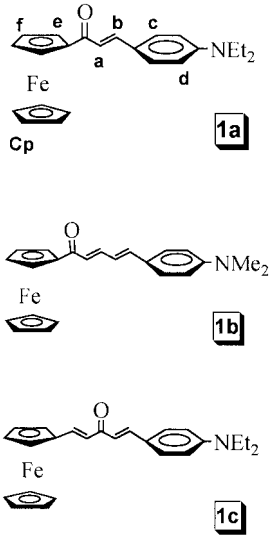

Scheme 1. Compounds **1a**–**c**.

common approach in this research field of ferrocenyl chemistry.

In this paper we report the X-ray and electrochemical characterization of the azacrown compound **2**, together with its cation electrochemical detection abilities. We describe the preparation and characterization of its protonated derivative [**2**H][BF_4] (**3**) and the investigation of thorough ^1H and ^{13}C NMR measurements concerning the interaction of compound **2** with calcium. In addition, we have recorded mass and IR spectral data that provide interesting information about the complex equilibrium that occurs during this interaction. Finally, we compare these results with those obtained in the previous study concerning the *N*-substituted methyl and ethyl compounds.[8] Furthermore, in agreement with experimental data, the theoretical MESP analysis of compounds **1a** and **2** indicates that both coordination sites of **2** are involved in this interaction process.

Results and Discussion

Synthesis and Characterization of Compound 2

We synthesized compound **2** by treatment of acetylferrocene with the appropriate crown aldehyde according to the improved procedure reported for **1a**–**c**[8] (Scheme 2). This new procedure allows a significant improvement on the isolated yield of **2** when compared to our original procedure.[2b] The product was isolated in good yield (65%) as a red powder. The IR spectrum of molecule **2** exhibits a ν(CO) stretching vibration at 1647 cm^{-1} in CH_3CN or in KBr. This low value is due to the conjugation of the CO bond with the double bonds of the π-system (-CH=CHC_6H_4- moiety) in the molecule.[2b,10a–10d] We could observe clearly both the characteristic strong stretching vibrations associated with the methylene groups of the crown in the 2873–2941 cm^{-1} range in CH_3CN[11a] and the asymmetrical stretching C–O–C vibrations as a broad band near 1125 cm^{-1}.[11b]

2D NMR experiments were undertaken in CD_3CN in order to provide a complete assignment of each signal (see Experimental Section). In comparison to compound **1a**, which has nearly the same signals in this solvent, the three CH_2 crown signals observed at δ = 3.57 (br. s), 3.62 (m), and 3.74 (t) ppm, respectively, appear as the ^1H NMR signature of the compound **2** (see Figure S1 in the Supporting Information). Interestingly, a low-field HMQC experiment allowed the verification of a clean correlation between the C_{ipso}-N carbon atom of the phenyl ring and the protons of the CH_2 crown groups α to the nitrogen atom (H_p). This feature is also observed for **1a** and **1c** between the C_{ipso}-N carbon atom and the protons of the CH_2 ethyl groups. Variable temperature NMR experiments in CD_3CN gave no further information.

Crystals of **2** suitable for X-ray structural analysis were obtained by slow recrystallization from CH_3CN. A perspective view of the molecule is shown in Figure 1, crystallographic data for compound **2** are provided in Table 1, and selected bond lengths and angles are listed in Table 2.

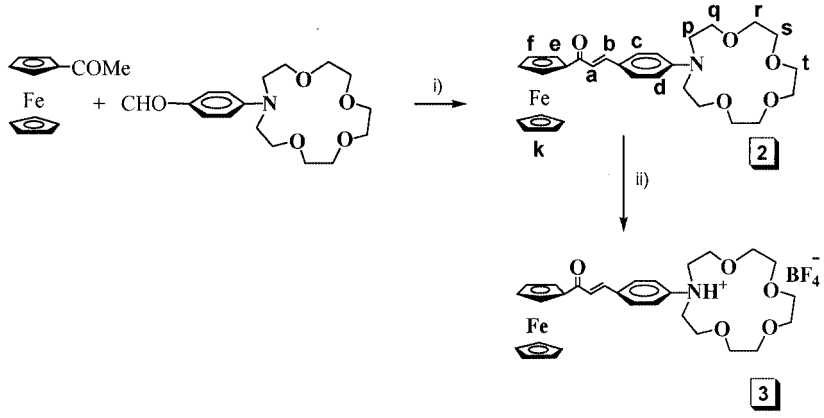

Scheme 2. Synthetic route to compounds **2** and **3**. Reagents and conditions: i) NaOH (5 equiv.), EtOH, 20 °C; ii) HBF_4 (1 equiv.), Et_2O, CH_3CN, 20 °C.

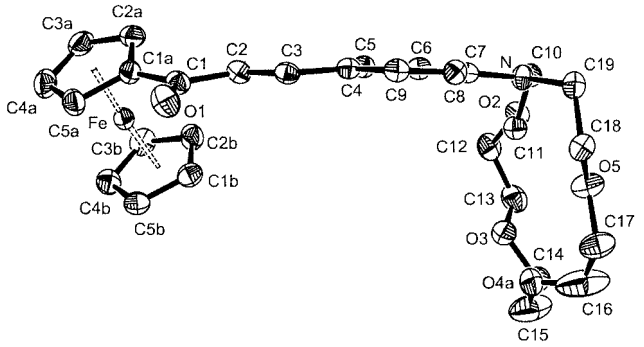

Figure 1.Molecular view of the structure of compound **2** (ORTEP 3) with 50% thermal ellipsoids.

Table 1. Crystallographic data for Compound **2**.

Empirical formula	$C_{29}H_{35}NO_5Fe$
Molecular mass	532.42
Crystal system	orthorhombic
Space group	*Pbca*
a [Å]	15.03434(9)
b [Å]	12.9933(8)
c [Å]	26.589(2)
V [Å^3]	5193.6(6)
$\rho_{calcd.}$ [mg m^{-3}]	1.362
Z	8
μ [mm^{-1}]	0.620
T [K]	160(2)
R_1 [$I > 2\sigma(I)$]	0.0381
wR_2 [$I > 2\sigma(I)$]	0.0850
R_1 (all data)[a]	0.0636
wR_2 (all data)[b]	0.0933

[a] $R_1 = \Sigma||F_o| - |F_c||/\Sigma|F_o|$. [b] $wR_2 = [\Sigma\{w(F_o^2 - F_c^2)^2/\Sigma[w(F_o^2)^2]\}]^{1/2}$.

Table 2. Selected bond lengths [Å] and angles [°] for compound **2** with esd's in parentheses.

Bond lengths [Å]		Bond angles [°]	
C1a–C(1)	1.477(4)	O(1)–C(1)–C(2)	122.6(3)
O(1)–C(1)	1.231(4)	O(1)–C(1)–C(1a)	120.3(3)
C(1)–C(2)	1.464(4)	C(2)–C(3)–C(4)	127.2(3)
C(2)–C(3)	1.339(4)	C(4)–C(5)–C(6)	122.1(3)
C(3)–C(4)	1.449(4)	C(6)–C(7)–C(8)	116.6(3)
C(4)–C(5)	1.403(5)	C(7)–C(8)–C(9)	121.3(2)
C(5)–C(6)	1.370(4)	C(6)–C(7)–N	121.5(3)
C(8)–C(9)	1.369(4)	C(8)–C(7)–N	121.8.(2)
C(7)–N	1.375(4)	N–C(10)–C(11)	114.0(2)
N–C(19)	1.462(4)	N–C(19)–C(18)	115.1(2)

The Cp rings of the compound are nearly eclipsed, with a tilt angle of 7°. The bond lengths within the ferrocenyl moieties[12] as well as the C=O, C_5H_4–C_1, and C=C distances compare well with values reported in the literature[12,13] and values obtained for the *N*-alkyl compounds **1b** and **1c**.[8] In compound **2**, the ethylenic bond is *cis* to the CO function, as for the two structurally characterized compounds **1b** and **1c**, and the conjugated organic chain is also almost planar. The crown moiety is essentially perpendicular to this link, with a torsion angle of 103° and 76° for C7–N–C10–C11 and C7–N–C19–C18, respectively. The observed disorder of the oxygen ring atoms illustrates the degree of flexibility of the crown moiety.[14] Its C–C and C–O distances are in the expected range of values.[15] To the best of our knowledge, this molecule is the fourth structurally characterized example of a monosubstituted compound presenting a $C_5H_4COCH{=}CHC_6H_4$ linkage.[8,12a] The C–N distance in **2** [1.375(4) Å] is close to the values observed for **1b**, **1c**, and $[(C_5H_5)Fe(C_5H_4COC_6H_4NH_2)]$[10d] [1.385(4), 1.384(5), and 1.368(9) Å, respectively]. As expected, these distances are longer than that in $[(C_5H_5)Fe(C_5H_4\text{-}COCH{=}CHC_6H_4NO_2)]$[12a] [1.224(11) Å], which bears an electron-withdrawing NO_2 function.

It is noteworthy that the C1a–N distance of around 9.0 Å is significantly shorter than in **1b** and **1c** (11.5 and 11.4 Å, respectively). The distance between the iron atom and the crown carbons (C11, C12) is approximately 9.5 Å. The shortest distance between the Cp unit and the crown ring is the C2B–C12 distance of 7.8 Å.

Electrochemical Studies: Characterization of Compound 2

The electrochemical properties of compound **2** were investigated in CH_3CN (Table 3) and a typical voltammogram of this species is shown in Figure 2. The shape of the cyclic voltammogram is not altered either by multiple successive scans or by change of the scan rate. As shown in Figure 2 and Table 3, compounds **1a** and **2** exhibit similar electrochemical characteristics. For these compounds the first wave observed in the cyclic voltammograms (CV), at $E_{pa} \approx 0.70$ V, is due to the oxidation of the ferrocene moiety and corresponds to a quasi-reversible process whose $E_{1/2}$ value was determined by linear voltammetry. The first irreversible oxidation process of compound **2**, whose $E_{1/2}$ value is 0.92 V, may be attributed to the oxidation potential of the organic amine moiety ($E_{1/2}$ Org).[8] Moreover, it lies in the range of values reported for the oxidation of some azaferrocenyl compounds.[16] Interesting studies on the oxidation of organic and ferrocenyl aromatic and aliphatic amines[17–20] and our previous results[1d,8] suggest that different and/or competitive mechanisms (e.g. amine protonation or radical coupling) may be responsible for the second and third well-defined irreversible organic oxidation waves situated at E_{pa} = 1.20 V and 1.65 V. In reduction, the single wave observed (E_{pa} = –1.76 V) is attributed to a reduction process mainly located on the CO function.

As illustrated by the first organic oxidation potential, the organic moiety of compound **2** is slightly more difficult to oxidize than that of **1a**. This is probably due to the presence of the electron-withdrawing oxygen atom, which decreases the donor strength of the nitrogen atom. Under similar conditions, the same phenomenon is also observed in the case of the organic compounds $[CHOC_6H_4NEt_2]$ and $[CHOC_6H_4\text{-}p\text{-aza-15-crown-5}]$. An anodic shift (60 mV) of the oxidation potential of the organic moiety is observed for the second compound when compared to the first one. It is noticeable that the E_{pa} value of the "CO" reduction process of **2** may vary but its $E_{1/2}$ is always very close to that of the *N*-alkyl compound **1a**.

Table 3. Selected electrochemical characteristics of compounds **1a** and **2** in CH_3CN.[a]

	Fe				Org		CO	
	E_{pa}	$E_{1/2}$ (P)	ΔE_p	RI_p	E_{pa}	$E_{1/2}$ (P)	E_{pa}	$E_{1/2}$ (P)
1a	0.70	0.64 (*52*)	63	1.0	0.92; 1.60	0.84 (*47*); 1.50 (*106*)	–1.78	–1.69 (*46*)
2	0.70	0.63 (*54*)	84	1.0	0.99; 1.20*; 1.65	0.92 (*37*); #; 1.50 (*47*)	–1.76	–1.67 (*47*)

[a] P, ΔE_P [mV]; $E_{1/2}$, E_{pa} [V]. $\Delta E_p = E_p$(backward) – E_p(forward) = $E_{pc} - E_{pa}$. $RI_p = |I_p(\text{backward})/I_p(\text{forward})| = |I_{Pred}/I_{Pox}|$. P = slope of the linear regression of $E = f(\log|i/i_d - i|)$. Org = oxidation processes of the organic part of the molecule. Conditions: [complexes] = 10^{-3} M; Pt electrode (1 mm diameter); scan rate in cyclic voltammetry: 100 mV s^{-1}, in linear voltammetry: 5 mV s^{-1}; solution of 0.1 M nBu$_4$NBF$_4$ in CH_3CN; reference electrode SCE. * = residual wave; # = $E_{1/2}$ not determined.

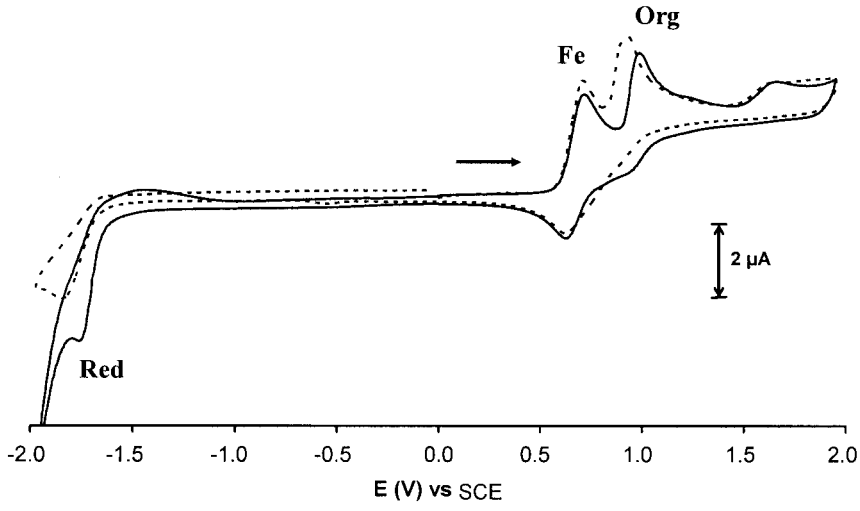

Figure 2. Cyclic voltammograms of compounds **1a** (dashed line) and **2** (solid line). Experimental conditions: Pt electrode (1 mm diameter) in 0.1 M solution of nBu$_4$NBF$_4$ in CH_3CN; scan rate 100 mV s^{-1}; ligand concentration 10^{-3} M; reference electrode SCE.

Electrochemical Calcium Recognition Ability of Compound 2

Electrochemical tests were first performed with **2** (10^{-3} M) in acetonitrile in the presence of various cations (Li^+, Na^+, K^+, Ba^{2+}, Mg^{2+}, Ca^{2+}, Cu^+, Cu^{2+}, and Zn^{2+}). Complex changes occurred in the presence of copper cations and give rise to unclear detections that have not been studied further. As for compound **1a**, compound **2** is poorly sensitive to the presence of cations other than Mg^{2+} and Ca^{2+}. The design of chemosensors that are specific to these biologically relevant cations is a challenging task for many groups.[21] However, for the Mg^{2+} cation, the detection was rather inefficient and peculiar: with one equivalent of salt the iron potential very slowly shifted anodically ($\Delta E_{1/2}$ = 50 mV after 2 h), whereas an incomplete decrease of the intensity of the organic wave was observed, even in salt excess.

As the Ca^{2+} electrochemical sensing was very clear for compound **2** we were especially interested in it. Addition of one equiv. of $Ca(OSO_2CF_3)_2$ to compound **2** induced a clear shift of the $Fe^{II/III}$ couple to anodic potential ($\Delta E_{1/2}$ = 70 mV; Figure 3). This shifted wave still corresponds to a quasi-reversible process ($E_{1/2}$ = 0.70 V, ΔE_p = 81 mV, R_{Ip} = 1.0). Simultaneously, the waves corresponding to the oxidation processes of the organic part of the molecule disappeared. The reduction process is also strongly perturbed (see Figure S2 in the Supporting Information): a very broad, ill-defined reduction wave could be observed around –0.8 V while a new reduction process appeared at –0.19 V (vide infra). Furthermore, when an equimolar mixture of Li^+, Na^+, K^+, Ba^{2+}, Zn^{2+} (4 equiv.) in the presence of 1 equiv. of Ca^{2+} was added to an acetonitrile electrochemical solution of **2**, the same electrochemical characteristics as those induced by Ca^{2+} alone were obtained.

The results obtained here are similar to those obtained for **1a** upon calcium addition. Consequently, in this family of compounds, the cation detection is more sensitive to the nature of the Fe–N spacer than to the nature of the aza group.

Upon comparing the reported data concerning the electrochemical detection of lithium by [(C_5H_5)Fe-$(C_5H_4CH{=}CHC_6H_4NMe_2)$][16] and by [$Fe(C_5H_4CONR_2)_2$][22] with the changes observed by cyclic voltammetry for compound **2** upon calcium addition, it appears that the Ca^{2+} complexation process could involve the whole organic part of molecule **2** since *both* its oxidation and reduction processes are entirely perturbed. Therefore, to determine in particular whether the azacrown moiety and/or the CO function were involved in this complexation (or interaction) process, a thorough NMR study was undertaken.

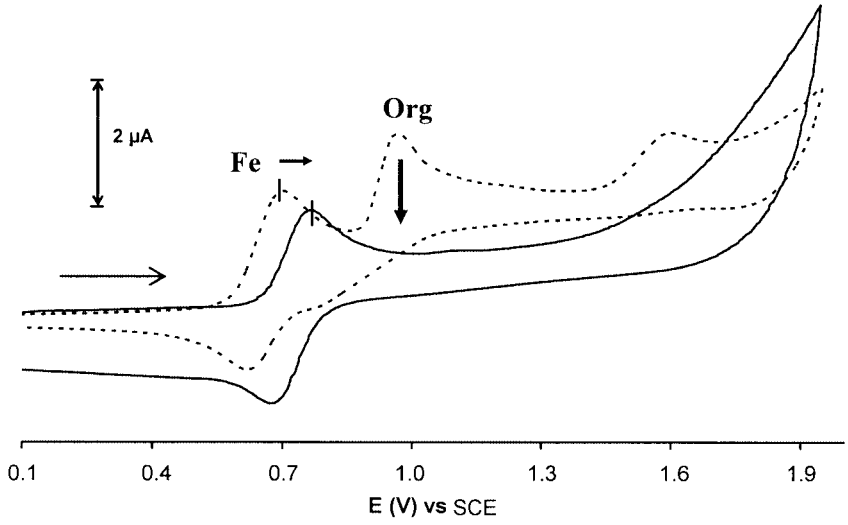

Figure 3. Segmented cyclic voltammograms of compound **2** (dashed line), and **2** + 1 equiv. of $Ca(OSO_2CF_3)_2$ (solid line). Experimental conditions: Pt electrode (1 mm diameter) in 0.1 M solution of nBu_4NBF_4 in CH_3CN; scan rate 100 mV s^{-1}; ligand concentration 10^{-3} M; reference electrode SCE.

NMR Spectroscopic Study: Treatment of Compound 2 with H^+ and Ca^{2+}

To investigate the complexation at the nitrogen atom, compound **2** was protonated. In CH_3CN, treatment of compound **2** with $HBF_4{\cdot}Et_2O$ in a 1:1 stoichiometry turned the solution from red to pink and afforded the protonated species [**2**H][BF_4] (**3**; Scheme 2). This new compound was isolated in good yield (80%). As described in the Experimental Section, elemental analyses and mass spectra are also in agreement with the proposed formula for **3**. In the solid state (IR spectrum, KBr), its elongation vibration ν(NH^+) could be located in the expected range 3030–3100 cm^{-1}.[1d,2b,23a]

The characterization of this compound was fully achieved by ^1H and ^{13}C 2D NMR measurements. In the ^1H NMR spectrum (CD_3CN, 293 K, 400 MHz) the protonation reaction was confirmed by the presence of a new signal at δ = 8.48 ppm attributed to the proton of the NH^+ group.[1d,23b] The NCH_2 crown protons α to the nitrogen atom H_p appear as a downfield-shifted multiplet (δ = 3.90 ppm) compared to **2**, as shown in Figure 4. The HMQC measurements indicated that the H_q and H_r protons of the crown groups are diastereotopic (see Experimental Section).

Tables 4 and 5 clearly highlight that compounds **2** and **1a** have a similar NMR behaviour towards protonation. However, the $\Delta(\delta CH_p)$ value of **2** is smaller than that of **1**, which is probably due to the flexibility of the crown moiety. Stronger perturbations of the phenyl ring of **2** are observed upon protonation: the $\Delta(\delta H_d)$ values are 1.16 ppm and 0.82 ppm for **2** and **1a**, respectively. For both compounds, the CH_d and C_{ipso}-C carbon shifts are also sensitive to the important structural variations that occur.[9] Finally, the CH_c, CH_e, CH_f, and CO groups present the smallest variations.

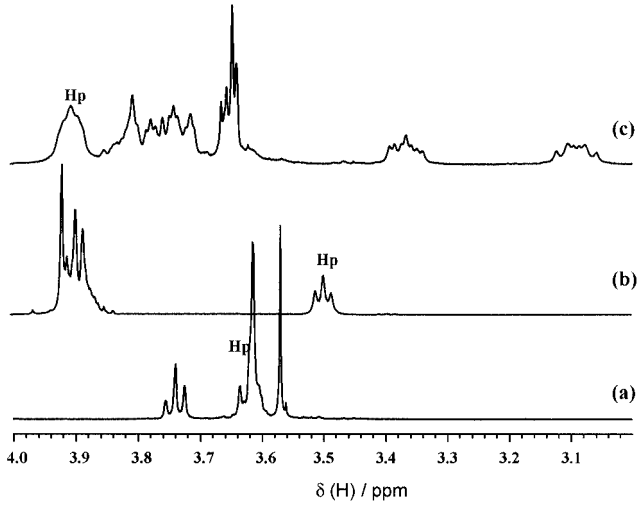

Figure 4. ^1H NMR (400 MHz, CD_3CN) spectra in the δ = 3.0–4.0 ppm range: crown region of (a) **2**, (b) **2** + 1 equiv. Ca^{2+}(c) **2** + 1 equiv. H^+.

Table 4. ^1H NMR (400.13 MHz, CD_3CN, 293 K) shift variations [$\Delta\delta$, in ppm] of selected groups of compounds **1a** and **2** upon a) protonation and b) calcium addition (1 equiv.). [L] = 5×10^{-3} M. See group labeling in Scheme 2.

	H_a	H_b	H_c	H_d	H_p[a]	H_e	H_f
a) Protonation							
1a	0.31	0.11	0.40	0.82	0.23	0.05	0.10
2	0.31	0.12	0.40	1.16	0.28	0.06	0.11
b) Calcium addition							
1a	–0.01	0.17	0.01	–0.02	0	0.11	0.09
2	0.11	–0.02	0.15	0.59	–0.15	0.06	0.11

[a] H_p: protons α to the N atom.

Table 5. ^{13}C NMR (100.62 MHz, CD_3CN, 293 K) shift variations [$\Delta\delta$, in ppm] of selected groups of compounds **1a** and **2** upon a) protonation and b) calcium addition (1 equiv.). [L] = 5×10^{-3} M. See group labeling in Scheme 2.

Compound	CH_a	CH_b	CH_c	CH_d	CH_p	CH_e	CH_f	CO	C_{ipso}-C	C_{ipso}-N
a) Protonation										
1a	8.46	–3.50	–0.07	11.62	9.96	0.35	1.01	–0.07	16.08	–11.84
2	7.92	–3.31	–0.15	12.21	5.94	0.33	0.92	–0.12	15.72	–13.92
b) Calcium addition										
1a	–1.07	2.67	0.71	0.03	0.07	0.68	1.16	2.77	–0.36	0.55
2	4.05	–0.44	–0.46	9.04	0.23	0.56	1.09	1.48	7.34	1.80

To get an insight into the ligand–Ca^{2+} interaction process responsible for the electrochemical detection of calcium, the ^1H NMR spectra of this compound were recorded in CD_3CN both with and without one equivalent of calcium salt. To properly ascertain the variations of the shift observed, 2D NMR measurements were also performed (see Experimental Section).

As indicated in Table 4, the H_a, H_c, and H_d protons of compound **2** present similar downfield shift variations upon addition of Ca^{2+} as those induced by protonation of **2**, but with smaller magnitudes. In addition, calcium addition induces drastic downfield shifts of the H_d aromatic protons and of the azacrown protons H_{q-t}, and an upfield shift for the H_p crown protons adjacent to the nitrogen atom (see Figure 4). This phenomenon has been previously ascribed to conformational changes resulting from Ca^{2+} crown complexation.[24] This is also reminiscent of the NMR behaviour of organic aza-15-crown-5 compounds[25] and of the ferrocenylazacrown compound $[(C_5H_4CH_2N(C_{12}H_{24}O_5)Fe(C_5H_4)]_2$[26] towards alkali or alkaline-earth metal cations.

Tables 4 and 5 also illustrate how alkyl compound **1a** and crown compound **2** behave differently upon addition of one equivalent of calcium. In particular, the noticeable differences for compound **2** are that (i) the H_p shift occurs, (ii) the H_b proton is not affected, and (iii) the CH_d carbon atoms are strongly perturbed whereas the CO group is only moderately perturbed. The observed shifts with a 1:1 stoichiometry suggest that a preferred azacrown interaction occurs but that a competitive CO interaction may also exist. The studies of the effect of salt concentration presented in the two following sections reinforce this interpretation.

Mass Spectrometry, IR Spectroscopy, and a Theoretical Approach

First, to confirm that strong enough interactions may exist between ligand **2** and the $Ca(OSO_2CF_3)^+$ unit, mass spectra were recorded with samples of **2** (10^{-2} M) containing 0.5, 1, 2, and 4 equivalents of salt, respectively. These mass measurements revealed peaks for the three following species **2**M, $(\mathbf{2})_2$M, and $\mathbf{2}M_2$, where M is the calcium salt (see Experimental Section). This also indicates that different adducts may be present in these mixtures.

In order to confirm further the above NMR hypothesis, complementary investigations were performed. For the IR studies, stepwise addition of Ca^{2+} to a solution of **1a** at the NMR concentration led to a decrease in the intensity of the ν(CO) vibration at 1647 cm^{-1} and to the appearance of a new band located at 1630 cm^{-1}. An excess of salt (up to 10 equiv.) increased the intensity of this new vibration at the expense of the original ν(CO) vibration of the free ligand, which still remained. This is consistent with the proposed equilibrium between the two main species: the free form **1a**, and its 1:1 complexed form [**1a**$Ca(OSO_2CF_3)_2$].[8] In this case, interaction of Ca^{2+} with the CO function classically induces the lowering of the wavenumber.

In contrast, addition of one equivalent of Ca^{2+} to a solution of the crown compound **2** first led to a decrease of its main ν(CO) vibration at 1647 cm^{-1} while a new band appeared at higher wavenumber (1655 cm^{-1}, see Figure 5, part a). This is consistent with a preferred N-crown complexation,[27] which decreases the force constant of the C_{ipso}-N bond and the resonance with the conjugated system, thus strengthening the ν(CO) vibration mode. Furthermore, protonation of **1** and **2** at the nitrogen site also induces a significant shift of the ν(CO) vibration mode to higher wavenumber (from 1647 cm^{-1} to 1659 cm^{-1}). These latter results strengthen our interpretation.

When more calcium salt was added, the main feature observed was the increase of a new broad band centered at 1640 cm^{-1}; the intensity of the band situated at 1655 cm^{-1} also increased slightly (see part b of Figure 5). This latter phenomenon may be interpreted as the result of the formation of one species where Ca^{2+} is now interacting with CO. It is also consistent with the formation of a $\mathbf{2}M_2$ adduct which could potentially interact at high salt concentration through both its CO and azacrown groups. In conclusion, the CO group acts here as a Ca^{2+} IR sensitive probe.

Thus, the IR studies show that Ca^{2+} interacts with both possible coordination sites of **2**. As shown below, this is supported by a comparative theoretical investigation of the molecular electrostatic potential (MESP) of compounds **2** and **1a**.

The gas-phase molecular electrostatic potential (MESP) was computed for the experimental geometries of **1a** and **2** at the B3PW91/6-31G** level. The MESP has been shown to be weakly sensitive to the level of calculation.[28] A MESP minimum value of –0.101 a.u. is obtained for **1a**. Part a of Figure 6 displays the MESP isosurface for a value of –0.080 a.u. There is a continuous negative MESP region formed by the joining of the two lone-pair regions of the oxygen atom of the carbonyl moiety. This suggests that the minima of the MESP are located near the lone pairs of the

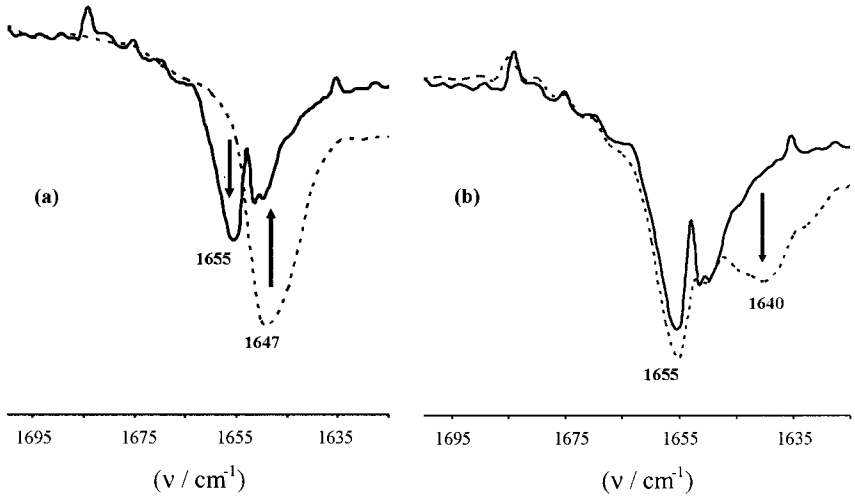

Figure 5. Segmented IR spectra of: (a) **2** (dashed line), **2** + 1 equiv. of $Ca(OSO_2CF_3)_2$ (solid line); (b) **2** + 1 equiv. of $Ca(OSO_2CF_3)_2$ (solid line), **2** + 4 equiv. of $Ca(OSO_2CF_3)_2$ (dashed line) in CH_3CN at NMR concentration.

oxygen atom of the carbonyl group. The carbonyl group is therefore expected to be the preferential binding site of the calcium cation. The picture is different for **2**. A similar MESP minimum value of –0.104 a.u. was computed at the same level. Again, the minima of the MESP are located near the lone pairs of the oxygen atom of the carbonyl group. However, as shown in part b of Figure 6, the lone pairs of the oxygen atoms of the crown moiety display a slightly less negative value of MESP than that of the carbonyl group. This suggests that these sites will now compete with CO for the calcium cation binding.

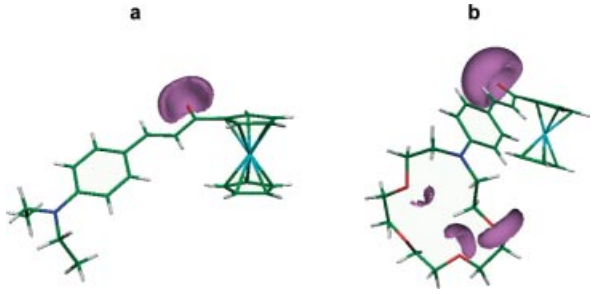

Figure 6. a) compound **1a**, MESP isosurface (–0.080 a.u.) and b) compound **2**, MESP isosurface (–0.055 a.u.), computed at the B3PW91/6-31G**level. Iron atom in sky-blue, nitrogen atom in deep blue, oxygen atom in red, and carbon atoms in green.

Analysis of the ^{13}C NMR Data and Proposition of a Ca^{2+} Interaction Model

To determine the number, the stoichiometry, and the values of the association constants of the calcium adducts involved, this interaction process was further studied by NMR spectroscopy. The variation of the ^1H and ^{13}C NMR chemical shifts was studied when changing the $Ca(OSO_2CF_3)_2$ concentration in CD_3CN. At 293 K, contrary to compound **1a**, the width of the ^1H NMR peaks observed for compound **2** was sometimes too great to allow an accurate assignment. Fortunately, the chemical shift variations of seven protons of **2** at 323 K could be successfully plotted against the calcium concentration. Figure 7 clearly illustrates a decreasing effect following the order $\Delta\delta H_d > \Delta\delta H_p > \Delta\delta H_c > \Delta\delta H_a > \Delta\delta H_b \approx \Delta\delta H_e, \Delta\delta H_f$, thereby corroborating a preferred crown complexation. It is noteworthy that the H_p protons are also the only protons of the crown ring whose shift variation can be clearly followed vs. the salt concentration at 323 K.

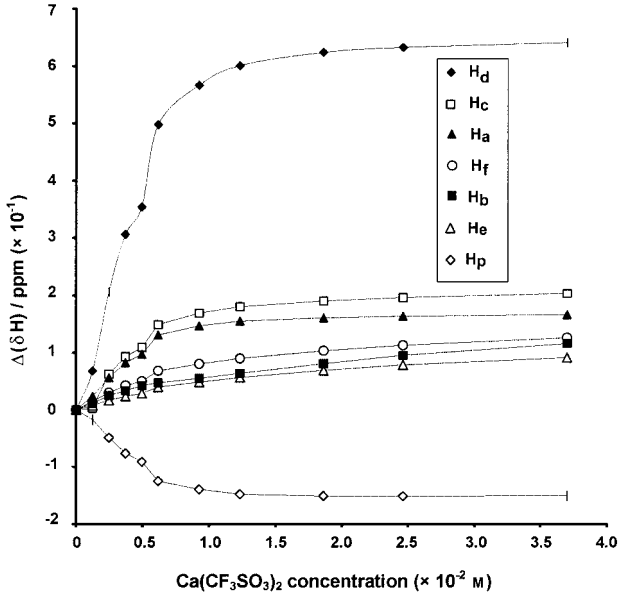

Figure 7. ^1H NMR chemical shift variations of the mentioned protons of **2** (6.2×10^{-3} M) vs. the $Ca(OSO_2CF_3)_2$ concentration in CD_3CN at 323 K. See atom labeling in Scheme 2.

At 293 K, as shown in Figure 8, the ^{13}C NMR study provides more information about the azacrown compound. As expected, the largest carbon shift variations occur for the CH_d and C_{ipso}-C carbons. The main feature is that the CO and the CH_b carbon shifts vs. Ca^{2+} concentration yield values larger than those observed for the CH_p groups involved in the crown complexation. This feature clearly indicates

that a Ca^{2+}–CO interaction also occurs.[4,8] Thus, Figures 7 and 8 illustrate clearly the resulting effect of a double-site interaction process that involves not only the crown ring but also the CO conjugated moiety. To the best of our knowledge, this is the first time that a thorough ^{13}C NMR investigation has shown the possibility of such a competitive process with a ferrocenyl ligand.

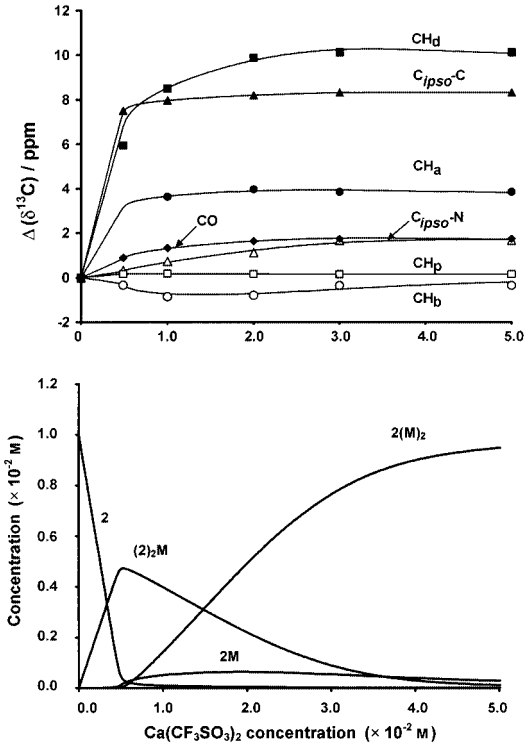

Figure 8. Top: ^{13}C NMR chemical shift variations of the mentioned protons of **2** (1×10^{-2} M) vs. the $Ca(OSO_2CF_3)_2$ concentration in CD_3CN at 293 K. Experimental values (dots) and calculated (lines) curves obtained by fitting the data. See atom labeling in Scheme 2. Bottom: Concentration of the formed species vs. calcium concentration. [**2**] = (1×10^{-2} M).

The continuous shifts of the sharp peaks observed during the calcium titration experiments are indicative of the presence of fast equilibria on the NMR timescale. So, for each calcium concentration, only a time-averaged spectrum of the ligand and/or the ligand–calcium complexes is observed. For example, in the ^{13}C NMR spectra, any observed chemical shift δC_i (where i corresponds to a specific site) is, in fact, a mole fraction weighted average of the shifts observed in the free and complexed molecules, see Equation (1).

$$\delta C_i = \sum(\delta C_{ij} X_j \alpha_j) = \delta C_i^{L} X_L + \delta C_i^{LM} X_{LM} + 2\delta C_i^{L2M} X_{L2M} + \delta C_i^{LM2} X_{LM2} \quad (1)$$

where L is the ferrocenyl ligand **2**, M is the calcium cation, and X the mole fraction of the considered species, and α_j its stoichiometric coefficient.The clear advantage of the global curve-fitting method, i.e. the simultaneous fitting of the data related to all signals, is that it can discriminate between several L_nM_m complex binding models.[29] We have previously reported the method used to determine the association constants for the different L_nM_m complexes present in solution.[30,31] In the present work, the fitted data were the δC_i for the seven curves shown in Figure 8. The following equilibria were considered and are described in the expressions below.

$$L + M \rightleftharpoons LM \qquad K_1$$

$$LM + L \rightleftharpoons L_2M \qquad K_2$$

$$LM + M \rightleftharpoons LM_2 \qquad K_3$$

In Figure 8, we display the ^{13}C NMR experimental data points together with the corresponding theoretical fit curves. A complete agreement between theory and experiment could only be obtained by taking into account the existence of three species [**2**M, (**2**)$_2$M, **2**M$_2$] of different stoichiometries and their corresponding association constants ($K_1 = 1.99\times10^3$, $K_2 = 8.09\times10^4$, $K_3 = 1.07\times10^3$ M^{-1}; values given with ±15% error). The other unknowns are the seven calculated δC_i values for each of the three species [**2**M, (**2**)$_2$M, **2**M$_2$] as indicated in Equation (1). Their adjusted $\Delta\delta C_i$ values are given in the Supporting Information (Table S6). The set of association constant values also gave a good curve fit in the case of the ^1H NMR spectroscopic data (see Figure S3). However, since the experimental temperature is different, the equilibrium can be modified. Therefore, this latter result must be considered with caution. As shown in Figure 8 (bottom), the calculated concentrations of the formed species vs. calcium concentration indicate that while (**2**)$_2$M is the main stoichiometry at low concentration, **2**M$_2$ is the major compound at high calcium concentration as for the alkyl compound **1c**.[8] Contrary to the alkyl compounds **1a**–**c**, (**2**)$_2$M may exist in significant amounts.

The model used to calculate the association constants does not make any distinction between the two sites of interaction – azacrown ring and unsaturated ligand CO system. However, association constants two to four orders of magnitude larger than for the alkyl compounds **1a**–**c** were found under the same experimental conditions.[8] The main difference is that these latter compounds do not interact through their nitrogen site. This suggests that the preferential complexation of the azacrown moiety stabilizes the formed adducts of **2**. It should be noted that for the **2**M compound, the calcium ion diameter of 1.98 Å closely fits the crown-ether cavity, which is 1.7–2.2 Å,[32] and the double charge of this cation promotes a good electrostatic interaction. This may explain the stability of such a complex. Considering a **L**$_2$M species, high values of the association constants have also been found for related *organic* ligands after treatment of their UV/Vis data.[30] In conclusion, in the range of ligand concentrations considered (from 6.2×10^{-3} to 1×10^{-2} M), several species compete. In a future paper, we will show that this NMR analysis is in full agreement with the results of a UV/Vis spectroscopic study realized with compound **2** and Ca^{2+}.

From a coordination point of view, as previously demonstrated, the Ca^{2+}–ligand interaction may occur with the crown moiety and/or with the unsaturated CO moiety. Con-

sidering first the CO–Ca^{2+} interaction, a screening of the CCDC database shows that the Ca^{2+} cation may interact with six to nine donor atoms of an organic ligand exhibiting a –C=C–C=O linkage.[33] Considering now the crown group, although numerous calcium-containing structures are known, the X-ray structures of only a few azacrown calcium complexes have been reported.[15,24,34] In these latter references, concerning purely organic ligands, the calcium is complexed to the crown moiety and the coordination shell of the calcium is completed (or not) with oxygen provided by another part of the organic ligand, or by a solvent molecule (methanol or water). Otherwise, a sandwich complex of Ca^{2+} with two 18-crown-5 ligands has been recently structurally characterized by Akutagawa et al.,[35] which suggests that a similar arrangement may exist for the $(\mathbf{2})_2$M azacrown compound. Moreover, under our experimental conditions, the triflate ion may also interact with the Ca^{2+} cation, for example through its O or F atoms, thereby increasing the number and nature of possible donor atoms and interacting modes.[36]

Unfortunately, it was not possible to obtain any X-ray structure of $\mathbf{2}Ca^{2+}$, but in the light of the above cited references[15,24,34–36] we may infer that several interacting formulations can be considered for one definite stoichiometry. For example, the $(\mathbf{2})_2$M species could be formed by interaction of two carbonyl groups of two different ligands with the same calcium, by interaction of one CO group of one ligand and one crown group of another ligand with calcium, or by sandwich complexation of calcium by two crown groups of different ligands.

As far as the $\mathbf{2}M_2$ species is concerned, the possibility of having two coordination sites of the same ligand simultaneously involved in the Ca^{2+} interaction, one located close to the negative site (CO) and the other to the positive (azacrown) site of **2**, is supported by the recent description of a dimeric X-ray structure of an interesting $[LPb^{2+}]_2$ chemosensor.[37]

In conclusion, to satisfy a required stoichiometry and to complete the calcium coordination sphere, one or both interacting sites, different anion binding modes, solvent molecules, or, if necessary, several ligands can be involved. However, in the reported equilibria, electrostatic interactions or weak intermolecular interactions (for example with adjacent phenyl groups), rather than classical complexation reactions, may also be considered. Finally, let us remark that the IR data corroborate the NMR analysis when increasing the Ca^{2+} concentration.

NMR tests were also performed with **2** in the presence of lithium, sodium, and potassium triflate, and showed weak proton-shift variations when compared to those due to the interaction with calcium (see Figures S4 and S5). Therefore, in these cases, a thorough NMR study was not appropriate. However, for example, the $\mathbf{2}Na^+$ adduct could be detected by mass spectrometry by a peak situated at m/z = 556 (FAB, and ES positive mode). For the $Ba(OSO_2CF_3)_2$ salt, a good ligand–Ba^{2+} interaction exists (see Figure S4) and the **2**M, $(\mathbf{2})_2$M, and $\mathbf{2}M_2$ species were detected by mass spectroscopy (ES). Because the Ba^{2+} electrochemical detection was not efficient, the **2**–Ba^{2+} interaction was not studied. As far as the Mg^{2+} cation is concerned, a thorough NMR study was not appropriate.

Pathway Between Calcium Interaction and Its Electrochemical Detection

In the above sections, we have shown that the protonation of ligand **2** affords the well-defined product **3**, whereas interaction of ligand **2** with calcium triflate affords different products (see also Figure 4). It must be pointed out that, in contrast, under our standard electrochemical conditions the protonated compound **3** leads to similar electrochemical characteristics as **2** in the presence of one equivalent of calcium triflate. In particular, for compound **3**, a new reduction wave at $E_{1/2}$ = –0.19 V (ΔE_p = 224 mV) was also clearly detected (vide supra), and is attributed to the NH^+ reduction process. How could these two different reactions − calcium interaction with ligand **2** and its protonation − lead to the same electrochemical characteristics (detection)?

In light of the outcome of the electrochemical detection of calcium by alkyl compounds **1a**–**c**,[8] we suspected a peculiar role of the nBu$_4$NBF$_4$ electrolyte in the $Ca(OSO_2CF_3)_2$ electrochemical detection. Therefore, for compound **2**, the calcium interaction process with $Ca(OSO_2CF_3)_2$ was re-examined in the presence of the nBu$_4$NBF$_4$ supporting electrolyte, following the same procedure as that detailed previously.[8] The main conclusion is that, as for the alkyl compounds **1a**–**c**, the three components in the mixture (Ca^{2+}, BF_4^-, H_2O) are responsible for the formation of the protonated species **3** (as a selected representative illustration see Figure 9). The small amount of water can be provided by the electrochemical or the NMR medium. There is no interaction between ligand **2** and the nBu$_4$NBF$_4$ electrolyte salt. In fact, the protonation reaction follows the $Ca(OSO_2CF_3)_2$ interaction process with ligand **2** only when the BF_4^- anion is present in the medium. Thus, in this case, the protonation reaction is the ultimate reaction step. Consequently, in the presence of the nBu$_4$NBF$_4$ electrolyte, the observed electrochemical calcium detection does not directly correspond to the $Ca(OSO_2CF_3)_2$ interaction process but is induced by it. The positive potential shift ($\Delta E_{1/2}$) of iron observed for ligand **2** upon Ca^{2+} addition corresponds, in fact, to that induced by ligand protonation. Thus, the $\Delta E_{1/2}$ of the Fe^{II}/Fe^{III} couple represents the difference of the oxidation potential between the protonated form [$Fe^{II}NH^+$] and the neutral form of the compound. For compounds **1a**–**c**, increasing the distance between the redox center and the amino site decreases the $|\Delta E_{1/2}|$ value of the Fe oxidation process. We have shown here with compound **2** that modifying the nature of the amine has no effect on the electrochemical detection. In fact, the C1–N distance in the new compound **2** is close to that of **1a**. According to the rule devised by Plenio et al.[38], the through-bond electronic communication along the conjugated chain responsible for the detection must be the same for **1a** and **2**, and is effec-

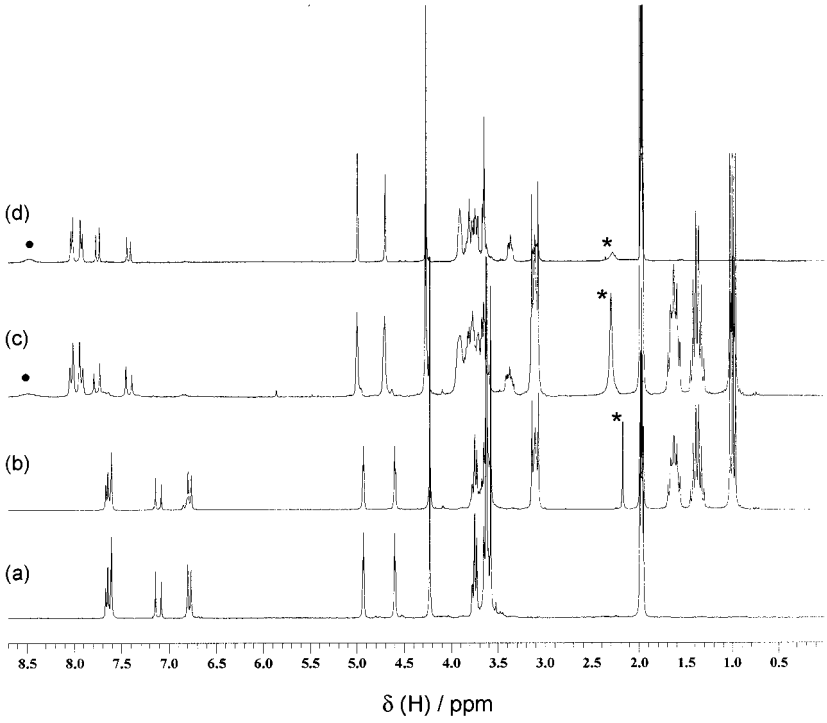

Figure 9. ^{1}H NMR (250 MHz, CD_3CN) spectra in the δ = 0–8.7 ppm range of (a) **2**, (b) **2** + 1 equiv. of nBu$_4$NBF$_4$, (c) mixture (b) + 1 equiv. of Ca(OSO$_2$CF$_3$)$_2$ after 4 h, (d) compound **3**. * H_2O, · NH^+.

tively better than that for **1b**,**c**, which have a longer C1–N distance. Our findings are also in agreement with those obtained for the Mg^{2+} electrochemical detection by compounds [(C_5H_5)Fe(C_5H_4CH=CHC_6H_4R)] (R = NMe_2 and N-azacrown-5), leading to the same $\Delta E_{1/2}$ value, and for which a through-bond electronic communication has been proposed.[39]

Concluding Remarks

We have evaluated the first structurally characterized ferrocenyl azacrown chalcone compound **2** for its electrochemical cation detection ability. A remarkable sensing of the Ca^{2+} cation is possible. This sensing relies on a complex interaction that involves not only the CO moiety of this receptor, as for its simple alkyl homologues **1a**–**c**, but also the azacrown ring, as evidenced by IR spectroscopy and MESP calculations. This interaction gives rise to the formation of three species of different stoichiometry in equilibrium in solution. This kind of phenomenon is not usual for ferrocenyl compounds. This was especially evidenced by experiments varying the ligand/cation concentration ratio and using different techniques such as mass spectrometry and IR and 2D NMR spectroscopy.

In our compounds the CO function plays a role as a coordination site for the interaction and does not interrupt the electronic communication between the terminal N donor and the ferrocenyl center, which can sense the variation of the electronic density. In contrast, the CO group can change the selectivity for the cation electrochemical detection. In fact, under our experimental conditions, the CO-free compound [(C_5H_5)Fe(C_5H_4CH=CHC_6H_4-*p*-aza-15-crown-5)] detects the Li^+[16] Na^+ and K^+[39] cations through crown–cation interactions with a magnitude of the cathodic shifts of 110, 60, and 20 mV, respectively, for the Fe^{II}/Fe^{III} couple. One reason for this difference may be that for compound **2** these N–cation interactions are weakened by the charge transfer due to the presence of the electron-withdrawing CO group. For compound **2**, in these cases, the CO–cation interactions are also probably too weak to be electrochemically detected or to promote the final protonation responsible their detection.

In comparison to the **2**–Ca^{2+} interactions, **2**–Ba^{2+} interactions are probably different because the Ba^{2+} cation is larger, has a lower charge density, and a preference for intermolecular associations. These kinds of interactions do not allow the final Ba^{2+} electrochemical detection by compound **2**. The stability of these **2**–Ba^{2+} interactions is demonstrated by the addition of the nBu$_4$NBF$_4$ supporting electrolyte, which does not induce any change of the NMR spectra.

Overall, regarding the field of ferrocenyl chemistry, we have reported solid evidence for a novel and rare example of a ligand–cation complex equilibrium. Furthermore, we have also shown that this new X-ray characterized ferrocenyl azacrown ligand leads to a peculiar and rather selective electrochemical calcium detection in which the CO function plays a key role. These results also clearly highlight that the Ca^{2+}detection or sensing by ligand **2** is not a simple Ca^{2+} molecular interaction or recognition process.

Experimental Section

Materials: Toluene and THF were distilled from over sodium/benzophenone, whereas pentane, dichloromethane, and CH_3CN (pure SDS) were distilled from over CaH_2 and stored under argon. EtOH (analytical grade, purex SDS) was simply degassed. [$(C_5H_5)Fe(C_5H_4COMe)$] (95%; Aldrich), [C_6H_5-*p*-aza-15-crown-5] (98%; Acros), and HBF_4 (54% in Et_2O; Aldrich) were obtained from the indicated suppliers. $Ca(OSO_2CF_3)_2$ (96%; Strem) was used without purification. $LiOSO_2CF_3$ (99%; Strem), $NaOSO_2CF_3$ (97%; Fluka), $Ba(OSO_2CF_3)_2$ (97%; Fluka), $KOSO_2CF_3$ (99%; Acros), $Zn(OSO_2CF_3)_2$ (98%; Aldrich), and $Mg(OSO_2CF_3)_2$ (98%; Fluka) were obtained as indicated. All these salts were dried under vacuum, weighed, and added to solution under an argon atmosphere. [$CHOCH{=}CHC_6H_4$-*p*-aza-15-crown-5] was prepared according to the published procedure.[40]

General Instrumentation and Procedures: All syntheses were performed under a nitrogen atmosphere using standard Schlenk tube techniques. IR spectra were recorded on a Perkin–Elmer GX FT-IR spectrophotometer. Samples were run as KBr pellets or in CH_3CN. Elemental analyses were carried out on a Perkin–Elmer 2400 B analyzer at the L. C. C. Microanalytical Laboratory in Toulouse. Mass spectra were obtained at the Service Commun de Spectrométrie de Masse de l'Université Paul Sabatier et du CNRS de Toulouse (fast atom bombardment, FAB>0; or desorption chemical ionization, DCI) were performed on a Nermag R 10-10H spectrometer. A 9 kV xenon atom beam was used to desorb samples from the 3-nitrobenzyl alcohol matrix. Other spectra were performed on a triple quadrupole mass spectrometer (Perkin–Elmer Sciex API 365) using electrospray as the ionization mode. The infusion rate was 5 μL min^{-1}. ^{1}H and ^{13}C NMR spectra were recorded on Bruker AC 200, AM 250, DPX 300, and AMX 400 spectrometers and are referenced to external tetramethylsilane. For 2D NMR experiments, the observation frequencies were in the range 400.13 MHz for ^{1}H and 100.62 MHz for ^{13}C.

Electrochemical Studies: Voltammetric measurements were carried out with a home-made potentiostat[41] using the interrupt method to minimize the uncompensated resistance (iR drop). Experiments were performed at room temperature in an airtight three-electrode cell connected to a vacuum/argon line. The reference electrode consisted of a saturated calomel electrode (SCE) separated from the solution by a bridge compartment filled with the same solvent and supporting electrolyte solution. The counter electrode was a platinum wire of about 1 cm^2 apparent surface. The working electrode was a Pt electrode (1 mm diameter). The supporting electrolyte [nBu$_4$NBF$_4$ (99%; Fluka electrochemical grade) or Et$_4$NBF$_4$ (99%; Aldrich)] was melted and dried under vacuum for one hour. All solutions measured were 1.0×10^{-3} M in the organometallic complex and 0.1 M in supporting electrolyte. The solutions were degassed by bubbling argon before experiments. With the above reference, a value of $E_{1/2}$ = 0.45 V vs. SCE was obtained for 1 mM ferrocene (estimated experimental uncertainty of ±10 mV). Cyclic voltammetry was performed in the potential range –2 to 2 V vs. SCE scanning from 0 toward 2 V/SCE for oxidation studies (and from 0 towards –2 V/SCE for reduction studies) at 0.1 V s^{-1}, at room temperature. Before each measurement, the electrode was polished with Emery paper (Norton A621). To calculate the half-wave potential ($E_{1/2}$), the method is as follows: a quasi-steady-state behavior (at Pt working electrode: 1 mm of diameter) was obtained by the use of linear voltammetry at 5 mV s^{-1}.

Proton NMR Titration Studies: Proton and carbon NMR titrations were typically performed as followed. A solution (500 μL) of the receptor in a deuterated solvent (10^{-2} M) was added with a microsyringe to NMR tubes containing the appropriate quantities of solid $Ca(OSO_2CF_3)_2$ under inert atmosphere, and the NMR spectrum of the receptor was monitored. The samples of calcium salt were prepared by evaporating the corresponding calculated volumes of a standard solution (10^{-2} M) in acetonitrile. Stability constants were evaluated from titration data using the method indicated in the text.

[$(C_5H_5)Fe(C_5H_4COCH{=}CHC_6H_4$-*p*-aza-15-crown-5)] (2): A mixture of [$(C_5H_5)Fe(C_5H_4COMe)$] and $CHOC_6H_4$-*p*-(aza-15-crown-5) (1:1; 0.66×10^{-3} M), and five equiv. of NaOH was dissolved in ethanol (15 mL) and stirred for 24 h at room temperature. The mixture was evaporated to dryness and the residue was dissolved in dichloromethane (10 mL). The solution was filtered off and the solvent evaporated to dryness (twice). The product was purified by column chromatography on alumina (eluent: pentane/CH_2Cl_2) and the obtained red phase was extracted with THF as eluent. After evaporation of the solvent, the product was washed with pentane (30 mL) and dried to afford the desired product as a deep orange powder in 65% yield. ^{1}H NMR (CD_3CN, 293 K): δ = 3.57 (m, 4 H, H$_t$), 3.62 (m, 8 H, H$_p$, H$_s$), 3.63 (m, 4 H, H$_r$), 3.74 (t, $^3J_{Hp,Hq}$ = 6.3 Hz, 4 H, H$_q$), 4.22 (s, 5 H, C_5H_5), 4.59 (t, $^3J_{He,Hf}$ = 1.9 Hz, 2 H, H$_f$), 4.93 (t, $^3J_{He,Hf}$ = 1.9 Hz, 2 H, H$_e$), 6.77 (d, $^3J_{Hc,Hd}$ = 9.0 Hz, 2 H, H$_d$), 7.11 (d, $^3J_{Ha,Hb}$ = 15.5 Hz, 1 H, H$_a$), 7.62 (d, $^3J_{Hc,Hd}$ = 9.0 Hz, 2 H, H$_c$), 7.63 (d, $^3J_{Ha,Hb}$ = 15.5 Hz, 1 H, H$_b$) ppm. ^{13}C{^{1}H} NMR (CD_3CN, 293 K): δ = 52.86 (CH$_p$), 68.48 (CH$_q$), 69.76 (CH$_e$), 69.78 (CH$_t$), 70.21 (C_5H_5), 70.30 (CH$_s$), 70.96 (CH$_r$), 72.63 (CH$_f$), 83.35 (C_{ipso}-C_5H_4), 112.05 (CH$_d$), 118.59 (CH$_a$), 122.84 (C_{ipso}-C), 130.64 (CH$_c$), 141.06 (CH$_b$), 150.00 (C_{ipso}-N), 192.50 (CO) ppm. IR (KBr): $\tilde{\nu}$ = 1522, 1553, 1577, 1610, 1647 (ν_{CO}), 2855–2946 cm^{-1} (ν_{CH}); (CH_3CN): 1521, 1579, 1609, 1647 (ν_{CO}), 2873–2941 cm^{-1} (ν_{CH}). MS (DCI): m/z = 534 [M + H]$^+$. $C_{29}H_{35}FeNO_5$: calcd. C 65.30, H 6.61, N 2.63; found C 65.42, H 6.54, N 2.70.

Interaction of One Equivalent of Ca^{2+} with Compound 2: ^{1}H NMR (CD_3CN, 293 K): δ = 3.47 (s, 4 H, Hp), 3.84–3.92 (m, 16 H, H$_q$, H$_r$, H$_s$, H$_t$), 4.25 (s, 5 H, C_5H_5), 4.70 (t, $^3J_{He,Hf}$ = 1.9 Hz, 2 H, H$_f$), 4.99 (t, $^3J_{He,Hf}$ = 1.9 Hz, 2 H, H$_e$), 7.22 (d, $^3J_{Ha,Hb}$ = 15.6 Hz, 1 H, H$_a$), 7.36 (d, $^3J_{Hc,Hd}$ = 8.8 Hz, 2 H, H$_d$), 7.61 (d, $^3J_{Ha,Hb}$ = 15.6 Hz, 1 H, H$_b$), 7.77 (d, $^3J_{Hc,Hd}$ = 8.8 Hz, 2 H, H$_c$) ppm. ^{13}C{^{1}H} NMR (CD_3CN, 293K): δ = 53.09 (CH$_p$), 68.38, 68.96, 69.03, and 69.86 (CH$_q$, CH$_r$, CH$_s$, and CH$_t$), 70.32 (CH$_e$), 70.58 (C_5H_5), 73.72 (CH$_f$), 81.11 (C_{ipso}-C_5H_4), 121.09 (CH$_d$), 122.84 (CH$_a$), 130.18 (C_{ipso}-C, CH$_c$), 140.62 (CH$_b$), 151.80 (C_{ipso}-N), 193.98 (CO) ppm.

[$(C_5H_5)Fe(C_5H_4COCH{=}CHC_6H_4$-*p*-aza-15-crown-5)H][$BF_4$] (3): $HBF_4{\cdot}Et_2O$ (1 equiv.) was slowly syringed into a stirred solution of **2** (0.19×10^{-3} M) in acetonitrile (10 mL). The light-protected mixture was stirred for 4 h. After solvent evaporation, the product was washed with diethyl ether (30 mL) and pentane (40 mL), and dried under vacuum. A violet powder was obtained in 80% yield. ^{1}H NMR (400 MHz, CD_3CN, 293 K): δ = 3.09 (m, 2 H, H$_q$), 3.37 (m, 2 H, H$_r$), 3.64 (m, 4 H, H$_s$), 3.72 (m, 2 H, H$_r'$), 3.74 (m, 4 H, H$_t$), 3.79 (m, 2 H, H$_q'$), 3.90 (m, 4 H, H$_p$), 4.26 (s, 5 H, C_5H_5), 4.70 (t, $^3J_{He,Hf}$ = 2.0 Hz, 2 H, H$_f$), 4.99 (t, $^3J_{He,Hf}$ = 2.0 Hz, 2 H, H$_e$), 7.42 (d, $^3J_{Ha,Hb}$ = 16.0 Hz, 1 H, H$_a$), 7,75 (d, $^3J_{Ha,Hb}$ = 16.0 Hz, 1 H, H$_b$), 7.93 (d, $^3J_{Hc,Hd}$ = 8.4 Hz, 2 H, H$_d$), 8,02 (d, $^3J_{Hc,Hd}$ = 8.4 Hz, 1 H, H$_c$), 8.48 (br. s, 1 H, NH$^+$) ppm. ^{13}C{^{1}H} NMR (100.6 MHz, CD_3CN, 293 K): δ = 58.80 (CH$_p$), 68.90 (CH$_s$), 69.12 (CH$_q$), 70.09 (CH$_e$), 70.43 (C_5H_5), 70.43 (CH$_t$), 70.59 (CH$_r$), 73.55 (CH$_f$), 81.40 (C_{ipso}-C_5H_4), 124.26 (CH$_d$), 126.51 (CH$_a$), 130.49 (CH$_c$), 136.08 (C_{ipso}-N), 137.75 (CH$_b$), 138.56 (C_{ipso}-C), 192.38 (CO) ppm. IR (CH_3CN): $\tilde{\nu}$ = 1516, 1597, 1608, 1659 (ν_{CO}), 2880–2942(ν_{CH}), 3052–3149 cm^{-1} (ν_{NH^+}). MS-FAB: m/z = 534 [M – BF_4]$^+$.

$C_{29}H_{36}BF_4FeNO_5$: calcd. C 56.07, H 5.84, N 2.25; found C 55.96, H 5.78, N 2.23.

Mass Spectrometry: Interaction of Compound 2 with Ca^{2+}: The samples used were those of the NMR titrations. MS (ES, CH_3CN): m/z = 287 [**2** + Ca^{2+}], 722 [**2**M – $CF_3SO_3^-$], 1060 [(**2**)M_2 – $CF_3SO_3^-$], 1255 [(**2**)$_2$M – $CF_3SO_3^-$].

Computational Details: The molecular electrostatic potential (MESP) has been extensively used by chemists for probing molecular structure and reactivities.[42] It is the potential generated by the molecular charge distribution as experienced by a positive charge. The topological analysis of the MESP, proposed by Gadre at al.,[43] is a very valuable tool for exploring the sites of reactivity of a molecule as well as their relative strengths. The deepest minimum in the MESP distribution can generally be taken as the most favorable position for an approaching positive charge. The minima in the MESP indicate localization of electron density and can be treated as potent sites of electrophilic attack. The molecular electrostatic potential (MESP) was computed for the experimental geometries at the B3PW91/6-31G** level using Gaussian98.[44] Visualization of the MESP isosurfaces was performed with molekel.[45]

Curve-Fitting Method: In the cited references 4, 8, 30, and 31, D. Lavabre has performed all the simulations and parametric adjustments by relying on his homemade software, SA version 3.

Crystallographic Study: Data were collected at low-temperature (160 K) on a four-circle Kappa CCD XCALIBUR diffractometer from Oxford Diffraction using graphite-monochromated Mo-K_α radiation (λ = 0.71073 Å) and equipped with a nitrogen low-temperature device (CRYOSET). Final unit-cell parameters were obtained by means of a least-squares refinement of 5768 reflections. The structure was solved by direct methods using SIR92[46] and subsequent Fourier maps. The model was refined by least-squares procedures on F^2 using SHELXL97[47] implemented in WinGX.[48] Atomic scattering factors were taken from the International Tables for X-ray Crystallography.[49] All hydrogen atoms attached to carbon were introduced at their idealized positions [d(CH) = 0.93 Å] and were refined using a riding model. They were given isotropic thermal parameters 20% higher than those of the atom to which they are attached. The oxygen atom O(4) was found to be statistically distributed over two sites and was refined accordingly. All non-hydrogen atoms were anisotropically refined, and the weighting scheme used in the last refinement cycles was $w = 1/[\sigma^2(F_o^2) + (aP)^2 + bP]$, where $P = (F_o^2 + 2F_c^2)/3$. For all compounds the criteria for a satisfactory complete analysis were the ratios of the root-mean-square shift standard deviation being less than 0.1 and no significant features in final difference Fourier maps. Drawing of the molecule was realized with the help of ORTEP3[50] with 50% probability displacement ellipsoids for non-hydrogen atoms.

CCDC-245554 contains the supplementary crystallographic data for this paper. These data can be obtained free of charge from The Cambridge Crystallographic Data Center via www.ccdc.cam.ac.uk/data_request/cif.

Supporting Information (see also the footnote on the first page of this article): Figure S1. The ^{1}H NMR spectra of compounds **1a** and **2** in the δ = 1–8 ppm range. Figure S2. The cyclic voltammogram of **2** after Ca^{2+} addition, in reduction. Figure S3. The calculated curves obtained by fitting the ^{1}H NMR spectroscopic data of compound **2** at 323 K. Figure S4. The compared NMR spectra of compound **2** with 1 equiv. of Li^+, Na^+, K^+, Ba^{2+} and Ca^{2+}, respectively. Table S5. The ^{1}H NMR shift variations of compound **2** upon addition of one equiv. of the indicated salts. Table S6 shows the calculated $\Delta\delta C_i$ values for the three species **2**M, (**2**)$_2$M, and **2**M_2. S7 shows the NMR shifts for the interaction of one equiv. of $Ca^{2+}$with compound **2**, in CD_3CN at 323 K.

Acknowledgments

The authors would like to thank CALMIP (calcul intensif en Midi-Pyrénées, Toulouse, France) for use of their computing facilities and Professor Gadre for fruitful discussions.

[1] For examples of redox-active molecules see: a) P. D. Beer, *Adv. Inorg. Chem.* **1992**, *39*, 79–157; b) P. D. Beer, J. Cadman, *Coord. Chem. Rev.* **2000**, *205*, 131–155; c) J. C. Medina, T. T. Goodnow, M. T. Rojas, J. L. Atwood, B. C. Lynn, A. E. Kaifer, G. W. Gokel, *J. Am. Chem. Soc.* **1992**, *114*, 10583–10595; d) B. Delavaux-Nicot, A. Bigeard, A. Bousseksou, B. Donnadieu, G. Commenges, *Inorg. Chem.* **1997**, *36*, 4789–4797 and references cited therein. For examples of fluorescent molecules see: e) A. Prasanna de Silva, H. Q. N. Gunaratne, T. Gunnlaugsson, A. J. M. Huxley, C. P. McCoy, J. T. Rademacher, T. E. Rice, *Chem. Rev.* **1997**, *97*, 1515–1566; f) A. Czarnik, *Fluorescent Chemosensors for Ion and Molecule Recognition*, ACS Symposium Ser. 538, Washington DC, **1993**; g) R. Y. Tsien, in *Methods in Cell Biology* (Eds.: D. Taylor, Y.-L. Wang), Academic Press, London, **1989**, vol. 30, 127.

[2] a) P. D. Beer, F. Szemes, V. Balzani, C. M. Salà, M. G. B. Drew, S. W. Dent, M. Maestri, *J. Am. Chem. Soc.* **1997**, *119*, 11864–11875; b) B. Delavaux-Nicot, S. Fery-Forgues, *Eur. J. Inorg. Chem.* **1999**, 1821–1825; c) S. Fery-Forgues, B. Delavaux-Nicot, *J. Photochem. Photobiol. A: Chem.* **2000**, *132*, 137–159.

[3] a) F. Sancenon, A. Benito, F. J. Hernandez, J. M. Lloris, R. Martinez-Manez, T. Pardo, R. Soto, *Eur. J. Inorg. Chem.* **2002**, 866–875; b) J. Gan, H. Tian, Z. Wang, K. Chen, J. Hill, P. A. Lane, M. D. Rahn, A. M. Fox, D. D. C. Bradley, *J. Organomet. Chem.* **2002**, *645*, 168–175.

[4] J. Maynadié, B. Delavaux-Nicot, S. Fery-Forgues, D. Lavabre, R. Mathieu, *Inorg. Chem.* **2002**, *41*, 5002–5004.

[5] For example: a) A. G. Nagy, S. Toma, *J. Organomet. Chem.* **1984**, *266*, 257–268; b) A. G. Nagy, *J. Organomet. Chem.* **1985**, *291*, 335–340; c) J. P. C. G. Dubosc, U. S. Patent, **1967**, 3,335,008; d) A. N. Nesmeyanov, G. B. Shulp'in, L. V. Rybin, N. T. Gubenko, M. I. Rybinskaya, P. V. Petrovkii, V. I. Robas, *J. Gen. Chem. USSR* **1974**, *44*, 1994–2001; e) S. Toma, A. Perjessy, *Chem. Zvesti* **1969**, *23*, 343–351; f) J. Boichard, J. P. Monin, J. Tirouflet, *Bull. Soc. Chim. Fr.* **1963**, *4*, 851–856.

[6] X. Wu, P. Wilairat, M.-L. Go, *Bioorg. Med. Chem. Lett.* **2002**, *12*, 2299–2302.

[7] A. Ferle-Vidovic, M. Poljak-Blazi, V. Rapic, D. Skare, *Cancer Biother. Radiopharm.* **2000**, *15*, 617–624.

[8] J. Maynadié, B. Delavaux-Nicot, D. Lavabre, B. Donnadieu, J. C. Daran, A. Sournia-Saquet, *Inorg. Chem.* **2004**, *43*, 2064–2077.

[9] M. C. Grossel, D. G. Hamilton, J. I. Fuller, E. Millan-Barios, *J. Chem. Soc., Dalton Trans.* **1997**, 3471–3477 and references cited therein.

[10] a) R. M. Silverstein, G. C. Bassler, T. C. Morril, in *Spectrometric Identification of Organic Compounds*, 4th ed., John Wiley & Sons, New York, **1981**, chapter 3, 117–118; b) P. D. Harvey, J. G. Sharman, *Can. J. Chem.* **1990**, *68*, 223–227; c) D. Prim, A. Auffrant, Z. F. Plyta, J. P. Tranchier, F. Rose-Munch, E. Rose, *J. Organomet. Chem.* **2001**, *624*, 124–130; d) M. Ansorge, K. Polborn, T. J. J. Müller, *Eur. J. Inorg. Chem.* **2000**, 2003–2009.

[11] a) R. M. Silverstein, G. C. Bassler, T. C. Morril, in *Spectrometric Identification of Organic Compounds*, 4th ed., John Wiley & Sons, New York, **1981**, chapter 3, p 107; b) R. M. Silverstein, G. C. Bassler, T. C. Morril, in *Spectrometric Identification of Organic Compounds*, 4th ed., John Wiley & Sons, New York, **1981**, chapter 3, p. 115.

[12] a) S. V. Lindeman, R. E. Bozak, R. J. Hicks, S. Husebye, *Acta Chem. Scand.* **1997**, *51*, 966–968; b) F. H. Allen, O. Kennard, D. G. Watson, L. Brammer, G. A. Orpen, R. Taylor, *J. Chem. Soc., Perkin Trans. 2* **1987**, *12*, S1–S19.
[13] a) H. Shottenberger, M. R. Buchmeiser, H. Angleitner, K. Wurst, R. H. Herber, *J. Organomet. Chem.* **2000**, *605*, 174–183; b) A. C. Bényei, C. Glidewell, P. Lightfoot, B. J. L. Royles, D. M. Smith, *J. Organomet. Chem.* **1997**, *539*, 177–186; c) E. Gyepes, T. Glowiak, S. Toma, *J. Organomet. Chem.* **1986**, *316*, 163–168.
[14] *Crown Compounds Toward Future Applications* (Ed.: S. R Cooper.), VCH Publishers, Inc., New York, **1992**.
[15] S. Itoh, H. Kumey, S. Nagatomo, T. Kitagawa, S. Fukuzumi, *J. Am. Chem. Soc.* **2001**, *123*, 2165–2175.
[16] M. P. Andrews, C. Blackburn, J. F. McAleer, V. D. Patel, *J. Chem. Soc., Chem. Commun.* **1987**, 1122–1124.
[17] S. D. Ross, M. Finkelstein, E. J. Rudd, *Anodic Oxidation*, Academic Press, New York, **1975**, vol. 32, chapter 8, p. 189.
[18] a) R. Prins, A. R. Koorswagen, A. G. T. G. Kortbeek, *J. Organomet. Chem.* **1972**, *39*, 335–344; b) R. Prins, *Mol. Phys.* **1970**, *19* 603–620.
[19] M. Spescha, N. W. Duffy, B. H. Robinson, J. Simpson, *Organometallics* **1994**, *13*, 4895–4904.
[20] N. W. Duffy, J. Harper, P. Ramani, R. Ranatunge-Bandarage, B. H. Robinson, J. Simpson, *J. Organomet. Chem.* **1998**, *564*, 125–131.
[21] a) A. Ajayaghosh, E. Arunkumar, J. Daub, *Angew. Chem. Int. Ed.* **2002**, *41*, 1766–1769; b) A. Chesney, M. R. Bryce, A. S. Batsanov, J. A. K. Howard, L. M. Goldenberg, *Chem. Commun.* **1998**, 677–678.
[22] P. D. Beer, H. Sikanyika, C. Blackburn, J. F. McAleer, *J. Organomet. Chem.* **1988**, *350*, C15–C19.
[23] a) H.-J. Bruegge, D. Carboo, K. von Deuten, A. Knöchel, J. Kopf, W. Dreissig, *J. Am. Chem. Soc.* **1986**, *108*, 107–112; b) R. M. Silverstein, G. C. Bassler, T. C. Morril, in *Spectrometric Identification of Organic Compounds*, 4th ed., John Wiley & Sons, New York, **1981**, chapter 3, p. 198.
[24] C. D. Hall, A. Leineweber, J. H. R. Tucker, D. Williams, *J. Organomet. Chem.* **1996**, *523*, 13–22.
[25] K. Rurack, J. L. Bricks, G. Reck, R. Radeglia, U. Resch-Genger, *J. Phys. Chem.* **2000**, *104*, 3087–3109.
[26] T.-Y. Dong, C.-K. Chang, C.-H. Cheng, K.-J. Lin, *Organometallics* **1999**, *18*, 1911–1922.
[27] M. C. Grossel, M. R. Goldspink, J. A. Hriljac, S. C. Weston, *Organometallics* **1991**, *10*, 851– 860.
[28] S. A. Kulkarni, S. R. Gadre, *Chem. Phys. Lett.* **1997**, *274*, 255–263.
[29] a) M. J. Hynes, *J. Chem. Soc., Dalton Trans.* **1993**, 311; b) L. Fielding, *Tetrahedron* **2000**, *56*, 6151–6170.
[30] N. Marcotte, S. Fery-Forgues, D. Lavabre, S. Marguet, V. G. Pivovarenko, *J. Phys. Chem. A* **1999**, *103*, 3163–3170.
[31] S. Fery-Forgues, D. Lavabre, D. Rochal, *New J. Chem.* **1998**, *22*, 1531–1538.
[32] a) C. J. Pedersen, H. K. Frendsdorff, *Angew. Chem. Int. Ed. Engl.* **1972**, *11*, 16–25; b) B. Dietrich, *J. Chem. Educ.* **1985**, *62*, 954–964.
[33] See, for example: a) T. Sato, H. Takeda, K. Sakai, T. Tsubomura, *Inorg. Chim. Acta* **1996**, *246*, 413–421; b) V.-C. Arunasalam, I. Baxter, S. R. Drake, M. B. Hursthouse, K. M. A. Malik, S. A. S. Miller, D. M. P. Mingos, D. J. Otway, *J. Chem. Soc., Dalton Trans.* **1997**, 1331–1335.
[34] J. Hu, L. J. Barbour, R. Ferdani, G. W. Gokel, *Chem. Commun.* **2002**, 1806–1807.
[35] T. Akutagawa, N. Takamatsu, K. Shitagami, T. Hasegawa, T. Nakamura, T. Inabe, W. Fujita, K. Awaga, *J. Mater. Chem.* **2001**, *11*, 2118–2124.
[36] a) G. A. Lawrance, *Chem. Rev.* **1986**, *86*, 17–33; b) A. D. Frankland, P. B. Hitchcock, M. F. Lappert, G. A. Lawless, *J. Chem. Soc., Chem. Commun.* **1994**, 2435–2436; c) A. Onoda, Y. Yamada, M. Doi, T. Okamura, N. Ueyama, *Inorg. Chem.* **2001**, *40*, 516–521.
[37] C.-T. Chen, W.-P. Huang, *J. Am. Chem. Soc.* **2002**, *124*, 6246–6247.
[38] H. Plenio, J. Yang, R. Diodone, J. Heinze, *Inorg. Chem.* **1994**, *33*, 4098–4104.
[39] P. D. Beer, C. Blackburn, J. F. McAleer, H. Sikanyika, *Inorg. Chem.* **1990**, *29*, 378–381.
[40] J. P. Dix, F. Vögtle, *Chem. Ber.* **1980**, *113*, 457–470.
[41] P. Cassoux, R. Dartiguepeyron, D. de Montauzon, J. B. Tommasino, P. L. Fabre, *Actual. Chim.* **1994**, *1*, 49–55.
[42] a) E. Sorocco, J. Tomasi, *Advances in Quantum Chemistry* (Ed.: P. O. Löwdin), Academic Press, New York, **1978**, vol. 11, 116 (115–193); b) E. Sorocco, J. Tomasi, in *Chemical Applications of Atomic and Molecular Electrostatic potentials* (Eds.: P. Politzer, D. G. Thruhlar), Plenum, New York, **1981**.
[43] a) S. R. Gadre, S. A. Kulkarni, I. H. Shrivastava, *J. Chem. Phys.* **1992**, *96*, 5253–5260; b) S. R Gadre, in *Computational Chemistry Reviews in Current Trends* (Ed.: J. Leczynski), World Scientific, Singapore, **1999**, vol. 4, p. 1; c) S. R. Gadre, R. N. Shirsat, in *Electrostatics of Atoms and Molecules*, Universities Press, Hyderabad, India, **2000**.
[44] M. J. Frisch, G. W. Trucks, H. B. Schlegel, G. E. Scuseria, M. A. Robb, J. R. Cheeseman, V. G. Zakrzewski, J. A. Montgomery Jr., R. E. Stratmann, J. C. Burant, S. Dapprich, J. M. Millam, A. D. Daniels, K. N. Kudin, M. C. Strain, O. Farkas, J. Tomasi, V. Barone, M. Cossi, R. Cammi, B. Mennucci, C. Pomelli, C. Adamo, S. Clifford, J. Ochterski, G. A. Petersson, P. Y. Ayala, Q. Cui, K. Morokuma, D. K. Malick, A. D. Rabuck, K. Raghavachari, J. B. Foresman, J. Cioslowski, J. V. Ortiz, A. G. Baboul, B. B. Stefanov, G. Liu, A. Liashenko, P. Piskorz, I. Komaromi, R. Gomperts, R. L. Martin, D. J. Fox, T. Keith, M. A. Al-Laham, C. Y. Peng, A. Nanayakkara, C. Gonzalez, M. Challacombe, P. M. W. Gill, B. Johnson, W. Chen, M. W. Wong, J. L. Andres, C. Gonzalez, M. Head- E. S. Gordon, J. A. Replogle, Pople, Gaussian 98, Revision A7, Gaussian, Inc., Pittsburgh PA, **1998**.
[45] P. F. Flükiger, S. Portman, Molekel 4.3, University of Geneva and CSCS/ETHZ, Switzerland, **2002**.
[46] SIR92, A program for crystal structure solution: A. Altomare, G. Cascarano, G. Giacovazzo, A. Guagliardi, *J. Appl. Cryst.* **1993**, *26*, 343–350.
[47] G. M. Sheldrick, SHELXL-97, *Program for the Refinement of Crystal Structures*; University of Göttingen, Göttingen, Germany, **1997**.
[48] WINGX 1.63 Integrated System of Windows Programs for the Solution, Refinement and Analysis of Single Crystal X-ray Diffraction Data: L. Farrugia, *J. Appl. Crystallogr.* **1999**, *32*, 837–838.
[49] International Tables for X-ray Crystallography, **1974**, vol. IV, Kynoch Press, Birmingham, England.
[50] ORTEP3 for Windows:L. Farrugia, *J. Appl. Crystallogr.* **1997**, *30*, 565.

Received: September 21, 2004

